Sustainable Structures
ISSN: 2789-3111 (Print); ISSN: 2789-312X (Online)
http://www.sustain-dpl.com/journal/sust
DOI: 10.54113/j.sust.2025.000077

ORIGINAL ARTICLE

Temperature effects on the compressive properties of wood-plastic composites

Bingyu Jian[a, b], Yijia Guo[c], Haitao Li[a, b, d, e, *], Yuanjie Li[f], Yana Jiang[b], Mahmud Ashraf[e, g], Jun Zhou[f]

[a] College of Civil Engineering, Nanjing Forestry University, Nanjing 210037, China
[b] Jiangsu Carbon Sequestration Materials and Structural Technology of Bamboo & Wood Research Center, Nanjing Forestry University, Nanjing 210037, China
[c] School of International Education, Tianjin Chengjian University, Tianjin 300384, China
[d] National-provincial joint engineering research center of biomaterials for MACHINERY PACKAGE, Nanjing Forestry University, Nanjing 210037, China
[e] Joint International Research Laboratory for Bio-composite Building Materials and Structures, Nanjing Forestry University, Nanjing 210037, China
[f] Jiangsu Qianyu WPC Technology Co., Ltd.,Yixing, 214200, China
[g] Deakin University, Geelong Waurn Ponds, VIC 3216, Australia.
*Corresponding author: Haitao Li, Professor, E-mail: lhaitao1982@126.com

Abstract: Wood-plastic composite (WPC) is made of plastic matrix, wood fiber or particles, compatibilizers and other modifiers. WPC has the appearance and strength of wood but offers toughness similar to plastics making it a suitable material for practical applications. In this paper, the influence of temperature on the compressive properties of two kinds of WPC specimens with equal size was studied, and the relationship between load displacement and stress strain of WPC composites at four kinds of temperatures was analyzed. It was found that with the increase of temperature, the mechanical properties of WPC decreased and the ultimate displacement increased. The relationship between the ultimate stress, the ultimate strain, the ultimate displacement and the temperature is analyzed, and the performance of the specimens with two sizes is compared. The reduction factor for strength in the Eurocode 5 and other references are compared with this paper, so as to provide a reference for the research in related fields.

Keywords: Polymer nanofiber, compression, mechanical properties, biomaterials

1 Introduction

Wood-plastic composites (WPCs) are high-performance materials fabricated by combining plant fibers (e.g., waste wood, crop straw) with plastics and additives through hot-pressing or melt extrusion processes. By integrating the renewability and biodegradability of plant fibers with the durability of plastics, WPCs serve as sustainable alternatives to conventional timber, alleviating the scarcity of forest resources. They are widely applied in construction, automotive, packaging, and decorative industries. Recent advancements have expanded the raw material scope to include diverse natural fibers, further enhancing their environmental benefits and application versatility. WPCs exhibit excellent mechanical properties and weather resistance, while their formulations can be tailored for specific functionalities (e.g., flame retardancy, mildew resistance), reducing plastic consumption and waste pollution. As eco-

Received: 24 November 2024; Received in revised form: 24 April 2025; Accepted: 2 May 2025

friendly materials, WPC production technologies are recognized as innovative and promising, aligning with sustainable development principles and advancing circular economies. **Fig. 1** shows WPC composite structures application examples such as gallery, outside wall, stairs, bus station and pavilion, which have been adopted in public facilities due to their durability and sustainability. While extensive research has focused on optimizing WPC performance, this study investigates the temperature effects on the compressive behavior of WPCs, aiming to understand their thermo-mechanical reliability for outdoor applications by using big test specimens.

(a) Wood-Plastic Composite gallery

(b) Wood-Plastic Composite wall and stairs

(c) Wood-Plastic Composite bus station

(d) Wood-Plastic Composite pavilion

Fig. 1 Some application examples of wood-plastic composite materials

Thermoplastics such as polyvinyl chloride (PVC), polypropylene (PP) and polyethylene (PE) are the most commonly used polymers used in WPC [1]. Waste products from both wood and plastic manufacturing industries such as high-density polyethylene recycled from packaging waste [2], plastics extracted from high pressure laminate (HPL), sand dust (filler) and waste thermoplastic from food barrel [3] can be used in WPC production. Hence, wider use of WPC would have singficant economic as well as environmental benefits. Compared with similar traditional materials, WPC has improved mechanical and physical properties, so it can replace similar traditional materials, especially in dry and hot environments [4].

The type and proportion of raw materials and the size of wood powder have been reported to affect the mechanical properties of WPC. Mertens et al. [5] reported that when the wood fiber content is 50% by wt., the strength performance of composite materials reaches the peak. Wood fibers with larger aspect ratio are suitable for producing high-performance WPC. Turku et al. [6] compared the mechanical properties of WPC prepared from spruce wood powder of three particle sizes and their results showed that the composite made from 20 mesh wood powder has better bending property. Chaudemanche, S. et al. [7] used the same batch of sawdust to produce wood flour with three particle size distributions. In general, the addition of large particles can improve the mechanical properties of WPCs. However, in the transverse extrusion direction, the properties of WPC can be enhanced by adding fine wood powder. Leu, S. et al. [8] found that the optimal concentration of coupling agent (maleic anhydride polypropylene) and lubricant (zinc stearate) in WPCs were both 3%. By adding a suitable amount of coupling agent, the mechanical properties of WPC can be improved.

The mechanical properties of WPC can be enhanced by pretreatment of raw materials. Lou et al.[9] used coconut shell fiber and polypropylene to make WPC, in which the weight of coconut shell was reduced by alkali treatment of coconut bran. Higher concentration and longer time of the alkali treatment produced WPCs with superior mechanical properties. Ma et al. [10] used alkali treatment and sol-gel method to modify the wood powder in-situ and prepared wood powder/silica hybrid, which was used as a reinforcing filler for polypropylene based WPC. It was found that WPC with mixed fillers had better mechanical properties. Islam, M.S. et al. [11] chemically pretreated wood with bendiazo salt, and then impregnated the monomer mixture in logs and treated wood samples with diazo salt. The results showed that PWPC had better mechanical and biological properties compared with untreated wood-plastic materials and raw materials. The mechanical and morphological properties of WPC can be significantly improved by pretreatment with 5% NaOH solution [12]. Before monomer treatment, Baysal, E. et al. [13] impregnated the mixture of boric acid (BA) and boric acid (BX) into wood at a concentration of 1%. The durability of WPC and flame retardant performance of wood can be enhanced by the mixed pretreatment of boric acid and boric acid.

Since WPC is mostly used outdoors, the environment has an important influence on the mechanical properties and durability of WPC. Therefore, it is necessary to study the influence of environmental factors such as temperature, weathering and light. Srubar, W.V. et al. [14] found that WPC with high fiber content, high moisture content and low tensile strength of polymer were most susceptible to freezing damage. The freezing resistance of WPC could be improved by using cork fiber (such as pine and spruce) and polymers with low modulus and high tensile strength. Delviawan et al. [15] used commercial wood powder of red pine to study the effects of particle size distribution and temperature on the mechanical properties of WPC. After 30 min wet grinding, the best mechanical properties were obtained under lyophilized conditions. The increase of temperature increased the moisture absorption rate and crystallinity of the specimen [16]. The discoloration during weathering can be significantly reduced by co-extrusion of high-density polyethylene (HDPE) layer on WPCs [17]. The thermal deformation temperature of thermosetting WPC composites can be improved by annealing treatment [18]. Xi, F. et al. [19] conducted the uniaxial compression test of WPC at seven temperatures and found that the uniaxial compressive strength and elastic modulus decreased with the increase of temperature. Lee, S.Y. et al. [20] observed that the flexural modulus and flexural strength of WPC were inversely related to temperature through cyclic hot-freezing test. At high temperatures, WPC begin to expand rapidly and then slowly contract until they reach equilibrium [21].

At present, reported research on WPC predominantly focuses on the optimization and modification methods of the formula, and the influence rule of external factors and the improvement method need more research. The current study investigates the compressive response of two types of WPCs (25 mm × 25 mm × 50 mm, 30 mm × 30 mm × 60 mm) when they are exposed to four different temperatures (60℃, 10℃, -10℃, -30℃). Observed changes in mechanical properties including load vs displacement, stress vs strain, elastic modulus, ductility coefficient and Poisson's ratio with temperature were carefully analyzed. Reduction factors for strength predictions were proposed based on the experimental results and the relevant comparisons with Eurocode 5 have been reported herein.

2 Materials and methods

The WPC used in this paper was made by Jiangsu Qianyu WPC Technology Co., LTD., with 40-80 mesh wood powder, high-density polyethylene and compatibilizer HDPE-G-mah, WPC ratio of 6.5:3.5. The production process involved mixing granulation followed by extrusion. 40 specimens considered in the current study were divided into 8 groups, with designation including the number of which is C, size symbol (I and II referring to 25 mm and 30 mm square cross-sections respectively), temperature and the specific number of the specimen as each group has 5 identical specimens. For example, CI10-1 represents the first specimen of size 25 mm × 25 mm × 50 mm tested at 10℃, whereas CII-10-1 represents the first specimen of size 30 mm × 30 mm × 60 mm loaded at -10℃. The sides of the specimen are marked as sides A, B, C and D in a counterclockwise direction. Vertical and transverse strain gauges were glued on to the midline of the four planes, and a symbol "×" was marked on the top surface. The relative humidity during the test was kept at 44%-74%. **Fig. 2** shows schematics as well as the real specimens with relevant specimen designations.

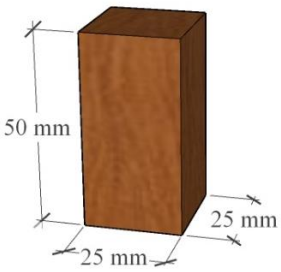

(a) The size of CI group

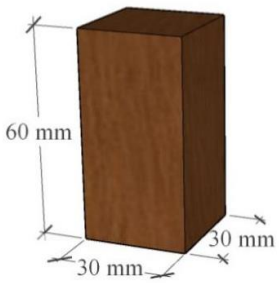

(b) The size of CII group

(c) CI group

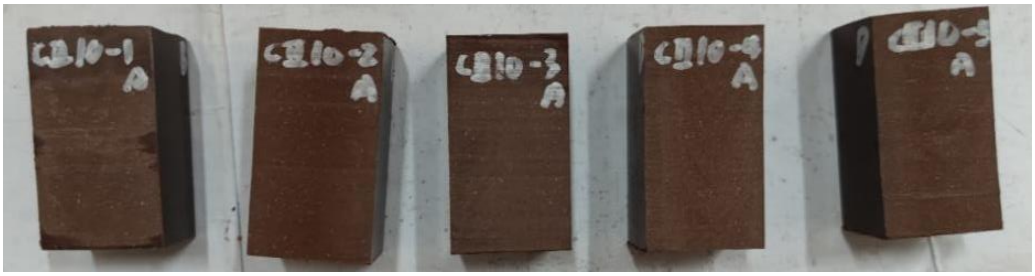

(d) CII group

Fig. 2 Specimens of two sizes

Table 1. shows the dimensions of all specimens and their corresponding temperatures and quantities.

Table 1. Specimens

Specimen	Cross section (mm× mm)	Height (mm)	Temperature (℃)	Quantity
CI60	25×25	50	60	5
CI10	25×25	50	10	5
CI-10	25×25	50	-10	5
CI-30	25×25	50	-30	5
CII60	30×30	60	60	5
CII10	30×30	60	10	5
CII-10	30×30	60	-10	5
CII-30	30×30	60	-30	5

The test device used in the study was WGDY-7350L universal mechanical testing machine with a temperature control box with range between -70 ~ 350℃. The specimens were placed within environmental chamber and were loaded under the controlled temperature. Four temperature conditions were set during the experiment, which were 60℃, 10℃, -10℃ and -30℃. TDS530 static data acquisition instrument was used to collect strain data at 10℃ and -10℃. Force control technique was used during the initial stages of loading and when the applied load reached approximately 80% of the ultimate load, the loading technique was changed to displacement control at a rate of 1.2 mm / s until the specimen failed. **Fig. 3** shows a schematic of the loading applied during the test.

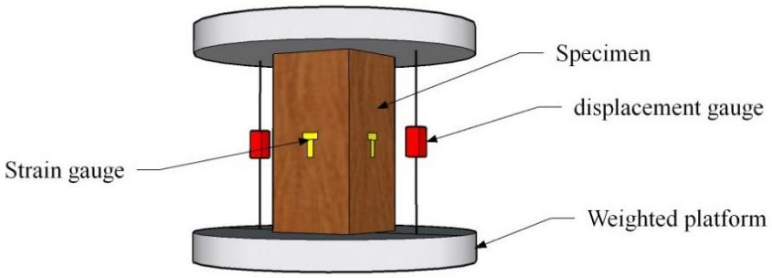

Fig. 3 Schematic diagram of loading

3 Analysis of Failure Modes

Failure modes of the tested specimens were carefully observed and they could be categorized into three broad categories such as Mode I - bidirectional splitting failure, Mode II - unidirectional splitting failure and Mode III - top surface failure. As an example, Mode I bidirectional splitting failure was observed in CII 10-5 specimen, as shown in **Fig. 4.**

(a) Face A (b) Face B (c) Face C (d) Face D (e) Top (f) Bottom

Fig. 4 Failure Mode I – bidirectional failure (CII10-5)

In bidirectional splitting failure, two cracks extended from the edge to intersect each other resulting in a Y or V shaped failure surface as shown in **Fig. 4a.** Load-displacement response was linear at the initial stage of loading and the specimen showed nonlinear elasto-plastic response after approximately 8 mins. The axial displacement kept increasing continuously showing obvious decrease in height of the specimen. Cracks began to appear at edges when the specimen reached around 80% of the ultimate load. As the load gradually increased, albeit at a slower rate, cracks began to propagate towards the centroid of the cross-section and finally cracks from opposing sides intersected each other causing failure of the specimen. The total duration of the test was approximately 10 minutes.

(a) Face A (b) Face B (c) Face C (d) Face D (e) Top (f) Bottom

Fig. 5 Failure Mode II – unidirectional failure (CI-30-2)

Fig. 5 shows a typical Mode II - unidirectional failure (Mode II) observed in specimenCI-30-2, in which a crack extended diagonally until it reached the adjacent/ opposite surface causing a complete failure of the specimen. Load-deformation response was similar to what was observed in Mode I type

failure i.e., initial linear stage continued up to 7-8 minutes and then gradually entered into a nonlinear regime, in which axial deformations were obvious prior to failure.

(a) Face A (b) Face B (c) Face C (d) Face D (e) Top (f) Bottom

Fig. 6 Failure Mode III – top surface failure (CII-10-1)

Fig. 6 shows a typical Mode III – top surface failure observed for specimen CII-10-1. Load deformation response was linear during the initial stages of loading and gradually moved to a nonlinear state somewhat earlier, at around 6 mins after the loading was applied, than the other two failure modes. Cracks appeared at one of the end surfaces and propagated along the height of the specimen until failure.

Table 2 shows the failure modes observed for of all specimens. It is obvious that diagonal cracks in Mode I and Mode II type failure were the most common type of failure. However, there was no specific correlation between temperature and failure modes.

Table 2. Failure type observed in tested specimens

Size of specimen	Temperature (℃)	Mode I	Mode II	Mode III	Total
I	60	2	2	1	5
	10	2	2	1	5
	-10	1	3	1	5
	-30	1	3	1	5
II	60	1	3	1	5
	10	4	1	0	5
	-10	2	2	1	5
	-30	2	2	1	5
Total	-	15	18	7	40

4 Results and Discussion

4.1 Analysis of load and displacement behavior

Fig. 7 shows the load - displacement relationships of the first group CI specimens with 25 mm square cross-sections. It is obvious that all specimens showed a linear relationship between load and displacement during early stages of loading with distinctly higher resistance at lower temperature. However, at -30℃ the specimens failed abruptly in contrast to the type of ductility observed in 60℃ and 10℃. There was very little difference in load-displacement response between 10 and -10℃ except some noticeable brittleness at -10℃.

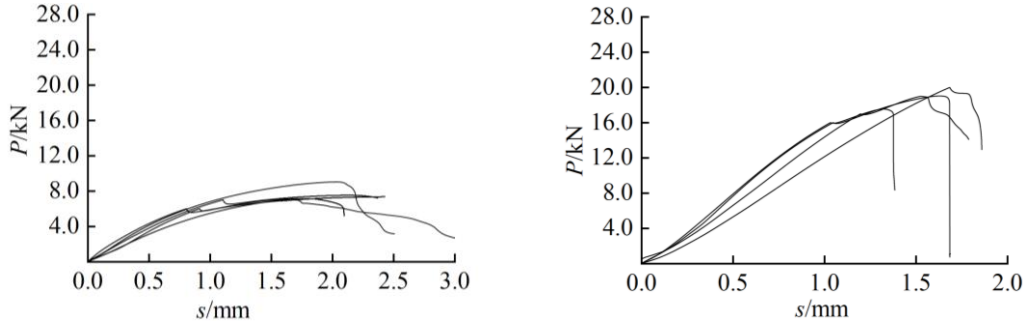

(a) CI60 (b) CI10

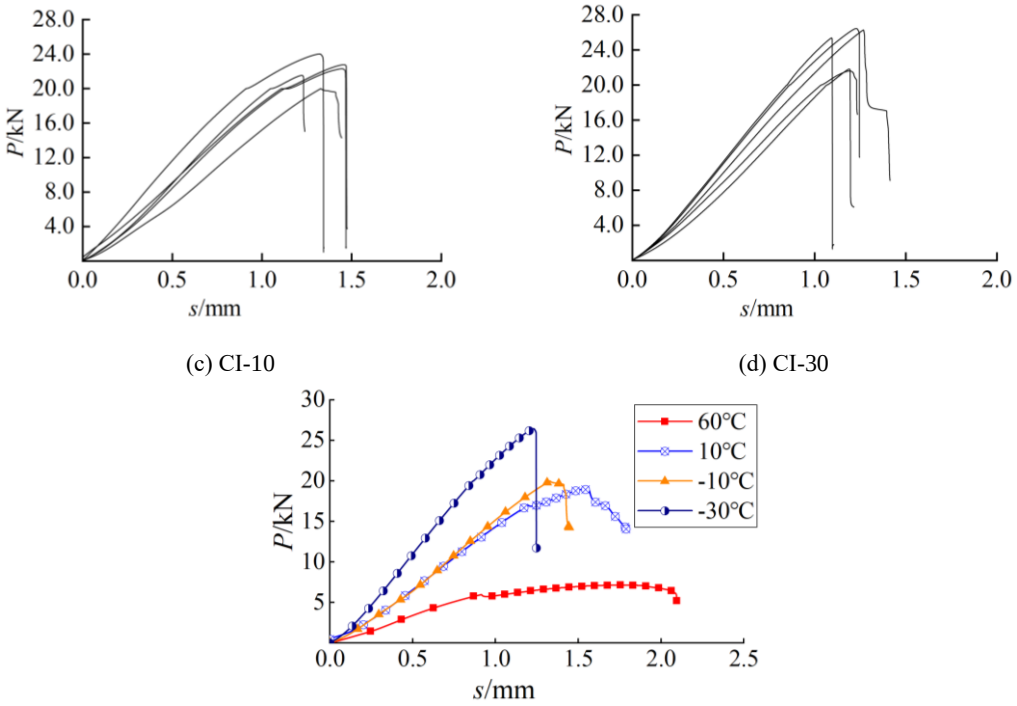

(c) CI-10 (d) CI-30

(e) Load-displacement curves at considered exposure temperatures

Fig. 7 Load-displacement response of CI (25 mm × 25 mm × 50 mm) specimens

Fig. 8 shows the load-displacement relationship of the first group of C Ⅱ specimens with 30mm square cross-section. Compared with the ductility type observed at -30℃ to 10℃, at 60℃, due to the higher temperature, the ultimate displacement increases and the ultimate load is significantly smaller than that at other temperatures. At -30℃ to 10℃, the specimen presents a linear change in the early loading stage and rapidly fails when it reaches the ultimate load. In general, the ultimate load decreases with the increase of temperature, a representative specimen of each size was selected for comparison as shown in **Fig. 8(e).**

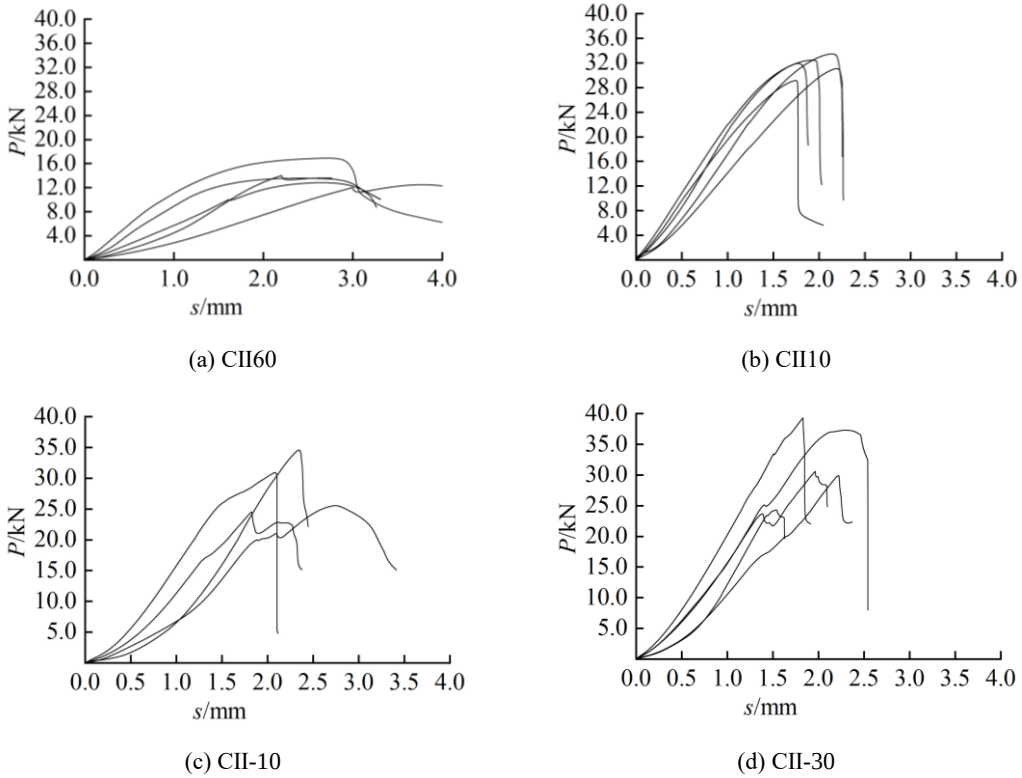

(a) CII60 (b) CII10

(c) CII-10 (d) CII-30

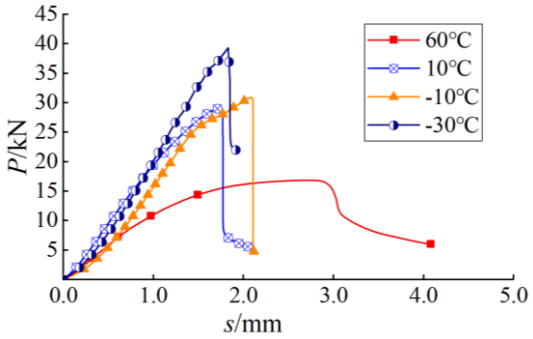

(e) Comparison of a group

Fig. 8 Load-displacement relationship of CII

4.2 Analysis of stress and strain

Fig. 9 shows the relationship between stress and axial strain of specimens under axial loads of 10℃ and -10℃. The trend of change can be divided into three parts: linear growth stage, with the increase of stress, the strain increases with the same proportion; Slope decreasing stage: when the limit stress reaches about 80%, the slope of the stress-strain curve decreases. Failure stage: after reaching the ultimate stress of the specimen, the bearing capacity of the specimen decreases rapidly until failure. Through comparative analysis, it is found that the elastic modulus of the specimen increases with the decrease of temperature, the specimen is less prone to deformation and the ultimate strain decreases.

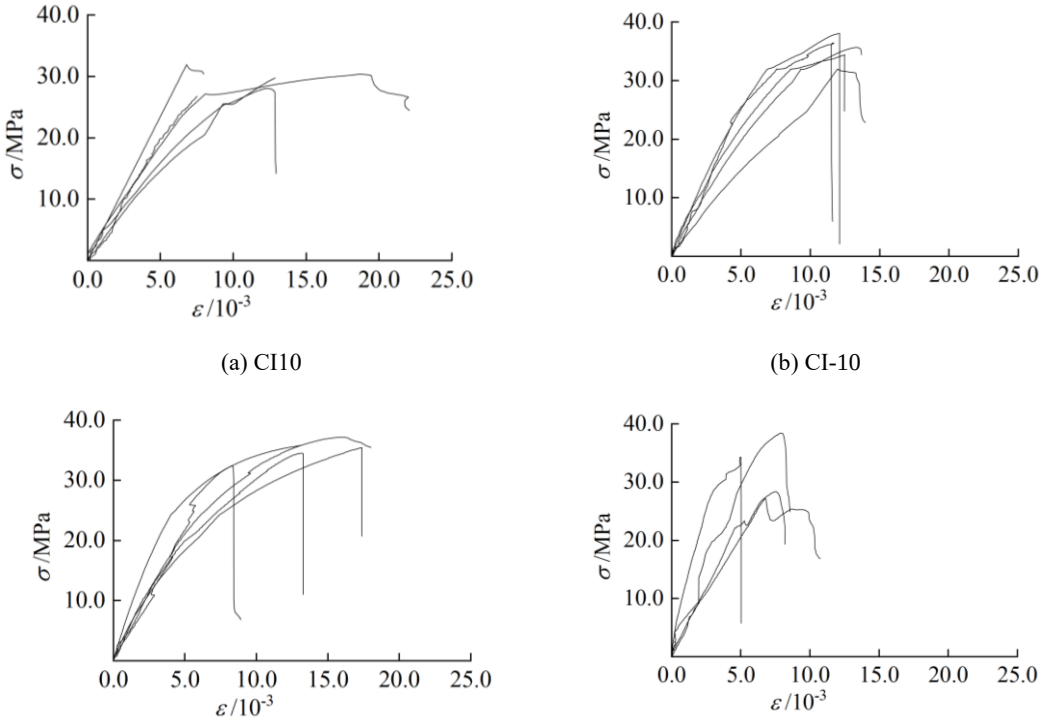

(a) CI10 (b) CI-10

(c) CII10 (d) CII-10

Fig. 9 Stress-strain relationship

4.3 Relationship between temperature and mechanical properties of WPC

Variation in mechanical properties of WPC specimens with change in temperature were analyzed using simple regression to identify any underlying trends.

Fig. 10 shows the variation of ultimate stress of the two groups of specimens under four temperatures considered in the current study. CI 25 mm square samples, showed a good linear trend

with temperature except for one outlier. In the case of 30 mm square CII group, all specimens seemed have reached the ultimate stress ~35 MPa at 10℃, and further reduction in temperature did not show any remarkable increase in the ultimate stress value.

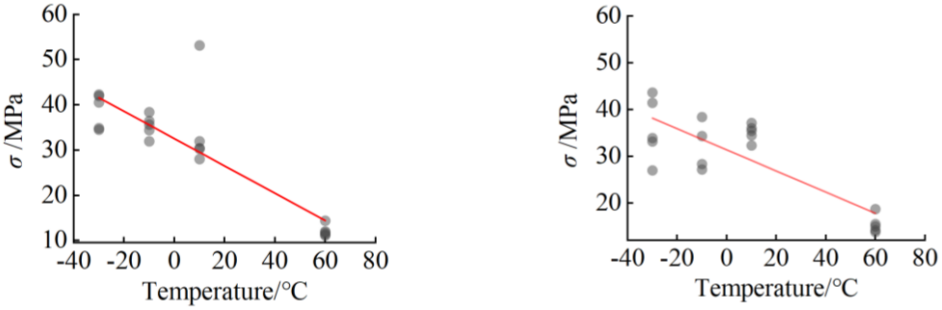

(a) CI (b) CII

Fig. 10 The relationship between temperature and ultimate stress

Regression analysis was conducted to develop some simple relationship between the ultimate stress σ_u (MPa) and temperature T (℃).

For CI (25 mm × 25 mm) groups: $\sigma = 32.57 - 0.30T$ $(R^2 = 0.72)$ (1)

In **Fig. 10(b)**, through regression analysis and calculation, the relationship between the ultimate stress and the ambient temperature of the specimen can be expressed by Equation (2): $\sigma = 31.41 - 0.23T$ $(R^2 = 0.66)$ (2)

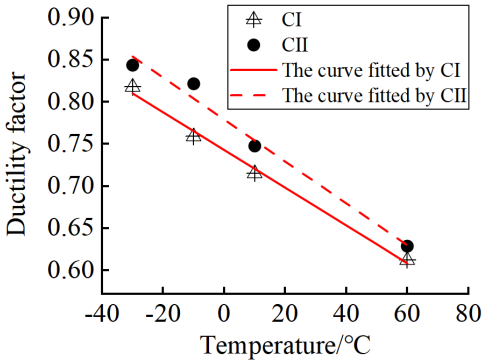

Fig. 11 Ductility factor and temperature

Table 3. Mechanical properties determined from test results

Temperature /℃	Specimen Group	E /MPa	σ /MPa	Poisson's ratio	Ductility factor	Specimen Group	E /MPa	σ /MPa	Poisson's ratio	Ductility factor
60	I		12.18		0.612	II	/	15.50		0.629
10		3857	34.80	0.369	0.715		5581	35.11	0.445	0.748
-10		4579	35.39	0.425	0.759		6429	32.09	0.489	0.822
-30			38.87		0.818		/	35.85		0.844

Note: Ductility factor is the ratio of ultimate displacement to yield displacement of specimen.

Fig. 11 shows the ductility factors of specimens with two sizes at different temperatures. It can be seen from the figure that the ductility factor of CII is larger than that of CI, and ductility factors of the two groups specimens are both linearly related to temperature. Through regression analysis and calculation, the relationship between the ductility factor and the temperature of CI can be expressed by Equation (3):

$$D = 0.743 - 0.00224T \ (R^2 = 0.99) \quad (3)$$

The relationship between the ductility factor and the temperature of CII can be expressed by Equation (4):

$$D = 0.779 - 0.00249T \ (R^2 = 0.98) \quad (4)$$

The test data are shown in **Table 3.**

4.4 Reduction factors for ultimate stress and ductility factor

Table 4 clearly shows that both the ultimate stress and the ductility factor of WPC samples became smaller as the temperature was increased from -30 ^{0}C to 60 ^{0}C. Calculated values for CI and CII were analyzed further to find relevant reduction factors to predict those relationships.

Fig. 12(a) and **(b)** shows the variation of the ultimate stress with respect to temperature increase for the two groups of specimens considered in the current study. It can be seen from the figure that the reduction factor of ultimate stress decreases roughly linearly with the increase of temperature. In **Fig. 10(a)**, through regression analysis and calculation, the relationship between the ultimate stress reduction factor and the temperature of the specimen can be expressed in Equation (5):

$$k = 0.91 - 0.0027T \ (R^2 = 0.99) \tag{5}$$

In **Fig. 12(b)**, through regression analysis and calculation, the relationship between the ultimate stress reduction factor and the temperature of the specimen can be expressed in Equation (6):

$$k = 0.87 - 0.0063T \ (R^2 = 0.82) \tag{6}$$

Fig. 12(c) and **(d)** shows the relationship between the reduction factors of ductility factors and temperature. It can be seen from the figure that the variation range of CII is larger than that of CI, and the reduction factors of the two groups specimens is roughly linear with temperature.

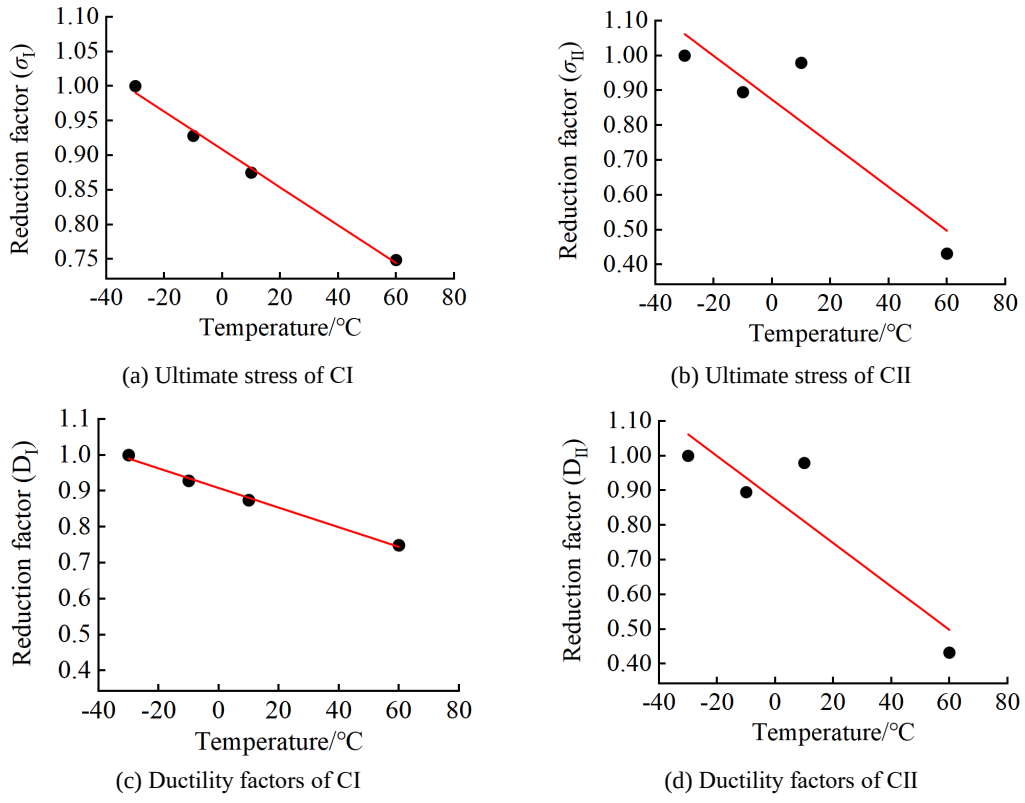

(a) Ultimate stress of CI

(b) Ultimate stress of CII

(c) Ductility factors of CI

(d) Ductility factors of CII

Fig. 12 Reduction factors and temperature

Through regression analysis and calculation, the relationship between the reduction factors of ductility factors and temperature of CI can be expressed in Equation (7):

$$k = 0.908 - 0.00274T \ (R^2 = 0.99) \tag{7}$$

The relationship between the ductility factor and the temperature of CII can be expressed by Equation (8):

$$k = 0.874 - 0.00626T \ (R^2 = 0.73) \tag{8}$$

The reduction factors of mechanical property of the two groups specimens are shown in **Table 4.** As can be seen from the table, with the increase of temperature, the elastic modulus, ultimate stress, Poisson's ratio and the reduction factor for ultimate load of most specimens all show a decreasing trend, and the reduction factor for ultimate load and ultimate stress has linear relationship with temperature.

Table 4. Reduction factors

Number	Reduction factor	-30℃	-10℃	10℃	60℃
I	E_c/E_{-10}	-	1.000	0.842	-
	v_c/v_{-10}	-	1.000	0.868	-
	σ_c/σ_{-30}	1.000	0.911	0.895	0.313
	f_c/f_{-30}	1.000	0.928	0.875	0.749
	μ_c/μ_{-30}	1.000	0.928	0.875	0.749
II	E_c/E_{-10}	-	1.000	0.868	-
	v_c/v_{-10}	-	1.000	0.910	-
	σ_c/σ_{-30}	1.000	0.895	0.979	0.432
	f_c/f_{-30}	1.000	0.974	0.886	0.745
	μ_c/μ_{-30}	1.000	0.974	0.886	0.745

Note: E is the elastic modulus, v is Poisson's ratio, σ is the ultimate stress, f is the ultimate load, μ is the ductility coefficient, the subscript is the temperature value, and the subscript c represents the corresponding specimen. For example, E_c/E_{-10} represents the ratio of the elastic modulus of the corresponding column to the elastic modulus of the specimen at -30℃.

The reduction factors proposed for strength in this paper were compared with those reported in previous studies [22] , [23], [19] and in Eurocode 5 [24], as shown in **Fig. 13.** Since the temperature of 20℃ is not set in this paper, the unit 1 of -30℃ is converted into 20℃, and the WPC [19] is converted into the same expression form. It can be seen from the figure that the line of bamboo scrimber [22] basically coincides with that of timber (Eurocode 5). The absolute value of the slope of the reduction factor of the fitted line in descending order is: WPC [19], CI in this paper, bamboo scrimber [22], timber (Eurocode 5), CII in this paper. When the temperature is above 20℃, the reduction factor from large to small is bamboo scrimber [23] (the horizontal grain is larger than the horizontal grain), timber (Eurocode 5), bamboo scrimber [22], CI, WPC [19] at the same temperature. In this paper, the data dispersion type of CII is relatively large, so it does not pass through the point (20,1) when fitting. [19] is also WPC, and its reduction factor changes with a high slope.

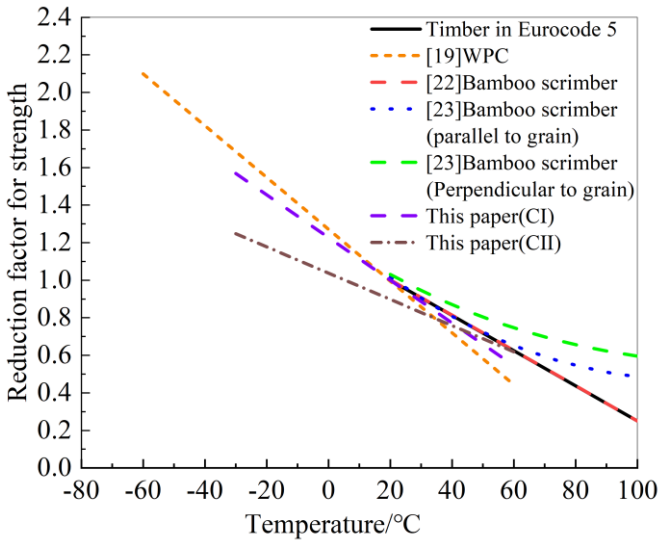

Fig. 13 Comparison of reduction factors for strength

5 Conclusions

In this paper, through the uniaxial compression test analysis of WPC of two sizes at room temperature, low temperature and high temperature, the following conclusions are obtained:

The uniaxial compression failure mode of WPC at low temperature and high temperature is basically consistent with the failure mode at room temperature. The main failure modes are bidirectional splitting failure, unidirectional splitting failure and top extrusion failure, and the first two are the main failure modes.

The experimental results showed that the compressive strength, elastic modulus, Poisson's ratio and displacement ductility factor of WPC decrease with the increase of temperature, and the ultimate displacement increases roughly with the increase of temperature.

Through the analysis of the mechanical properties of the two equally proportional volumes, it can be seen that the elastic modulus, Poisson's ratio and ductility coefficient of the large volume are larger than those of the small volume, the law of ultimate stress and displacement is not obvious.

By comparing the reduction factor for strength of this paper and some references with the Eurocode 5, it can be seen that with the increase of temperature, the ultimate stress of a bamboo scrimber decreases slowly, that of perpendicular to grain is greater than the that of parallel to grain, and both are smaller than the cork parallel to grain, the reduction speed of WPC is greater than that of Eurocode 5.

Acknowledgement

The writers gratefully acknowledge Yukun Tian, Chen Chen, Ben Chen, Shaoyun Zhu, Liqing Liu, Dunben Sun, Jing Cao, Yanjun Liu, Junhong Xu and others from the Nanjing Forestry University for helping.

Funding Statement

This work was supported by the National Natural Science Foundation of China (No. 51878354), the Natural Science Foundation of Jiangsu Province (No. BK20181402), Forestry Science and Technology Innovation and Promotion Project of Jiangsu Province (No. LYKJ[2024]08), 333 talent high-level projects of Jiang-su Province. Any research results expressed in this paper are those of the writer(s) and do not necessarily reflect the views of the foundations.

CRediT authorship contribution statement

Bingyu Jian: Investigation, Formal analysis, Writing – original draft. **Yijia Guo**: Investigation, Formal analysis, Writing – original draft. **Haitao Li**: Conceptualization, Funding acquisition, Supervision, Investigation, Formal analysis, Writing – original draft. **Yuanjie Li**: Supervision, Writing – review & editing. **Yana Jiang:** Investigation, Writing – review & editing. **Mahmud Ashraf**: Supervision, Writing – review & editing. **Jun Zhou**: Supervision, Writing – review & editing.

Conflicts of Interest

The authors declare that they have no conflicts of interest to this work.

Data Availability Statement

The datasets generated and analysed during the current study are available from the corresponding author on reasonable request.

References

[1] Friedrich, D., Thermoplastic moulding of Wood-Polymer Composites (WPC): A review on physical and mechanical behaviour under hot-pressing technique. Composite Structures, 2021, 262, 113649. https://doi.org/10.1016/j.compstruct.2021.113649

[2] Sommerhuber, P.F., J. Welling and A. Krause, Substitution potentials of recycled HDPE and wood particles from post-consumer packaging waste in Wood‐Plastic Composites. Waste Management, 2015, 46, 76-85. https://doi.org/10.1016/j.wasman.2015.09.011

[3] Huang, Y., et al., Eco-friendly wood-plastic composites from laminate sanding dust and waste poly(propylene) food pails. Waste Management, 2022, 149, 96-104. https://doi.org/10.1016/j.wasman.2022.06.012

[4] Elmushyakhi, A., Parametric characterization of nano-hybrid wood polymer composites using ANOVA and

regression analysis. Structures, 2021, 29, 652-662. https://doi.org/10.1016/j.istruc.2020.11.069

[5] Mertens, O., et al., Performance of thermomechanical wood fibers in polypropylene composites. Wood Material Science & Engineering, 2020, 15(2), 114-122. https://doi.org/10.1080/17480272.2018.1500494

[6] Turku and Karki, Reinforcing wood-plastic composites with macro- and micro-sized cellulosic fillers: Comparative analysis. Journal of Reinforced Plastics and Composites, 2013, 32(22), 1746-1756. https://doi.org/10.1177/0731684413496574

[7] Chaudemanche, S., et al., Properties of an industrial extruded HDPE-WPC: The effect of the size distribution of wood flour particles. Construction and Building Materials, 2018, 162, 543-552. https://doi.org/10.1016/j.conbuildmat.2017.12.061

[8] Leu, S., et al., Optimized material composition to improve the physical and mechanical properties of extruded wood–plastic composites (WPCs). Construction and Building Materials, 2012, 29, 120-127. https://doi.org/10.1016/j.conbuildmat.2011.09.013

[9] Lou, et al., Compatibility and mechanical properties of maleicanhydride modified the wood plastic composite. Journal of Reinforced Plastics & Composites, 2013, 32(11), 802-810. https://doi.org/10.1177/0731684413480250

[10] Ma, Y., et al., In situ fabrication of wood flour/nano silica hybrid and its application in polypropylene‐based wood‐plastic composites. Polymer Composites, 2020, 41(2), 573-584. https://doi.org/10.1002/pc.25389

[11] Islam, M.S., et al., Effect of coupling reactions on the mechanical and biological properties of tropical wood polymer composites (WPC). International Biodeterioration & Biodegradation, 2012, 72, 108-113. https://doi.org/10.1016/j.ibiod.2012.05.019

[12] Saiful Islam, M., et al., The effect of alkali pretreatment on mechanical and morphological properties of tropical wood polymer composites. Materials & Design, 2012, 33, 419-424. https://doi.org/10.1016/j.matdes.2011.04.044

[13] Baysal, E., et al., Some physical, biological, mechanical, and fire properties of wood polymer composite (WPC) pretreated with boric acid and borax mixture. Construction and Building Materials, 2007, 21(9), 1879-1885. https://doi.org/10.1016/j.conbuildmat.2006.05.026

[14] Srubar, W.V., An analytical model for predicting the freeze–thaw durability of wood–fiber composites. Composites Part B: Engineering, 2015, 69, 435-442. https://doi.org/10.1016/j.compositesb.2014.10.015

[15] Delviawan, A., et al., The effect of wood particle size distribution on the mechanical properties of wood–plastic composite. Journal of Wood Science, 2019. 65(1). https://doi.org/10.1186/s10086-019-1846-9

[16] Kamau-Devers, K., Z. Kortum and S.A. Miller, Hydrothermal aging of bio-based poly(lactic acid) (PLA) wood polymer composites: Studies on sorption behavior, morphology, and heat conductance. Construction and Building Materials, 2019, 214, 290-302. https://doi.org/10.1016/j.conbuildmat.2019.04.098

[17] Matuana, L.M., S. Jin and N.M. Stark, Ultraviolet weathering of HDPE/wood-flour composites coextruded with a clear HDPE cap layer. Polymer Degradation and Stability, 2011, 96(1), 97-106. https://doi.org/10.1016/j.polymdegradstab.2010.10.003

[18] Haider, A., et al., Melamine-resin based Wood Plastic Composites (WPC) - heat resistance. European Journal of Wood & Wood Products, 2009, 67(1), 71-76. https://doi.org/10.1007/s00107-008-0288-7

[19] Xi, F. and L. Zhao, Experimental study of the compressive properties of a wood–plastic composite at different temperatures. Polymer Composites, 2022, 1-7. https://doi.org/10.1002/pc.26815

[20] Lee, S.Y., et al., Mechanical Properties of Wood Flour Polypropylene Composites: Effect of Cycled Temperature Change. Elastomers and Composites, 2011, 46(3), 218-222. https://doi.org/10.7473/EC.2011.46.3.218

[21] Yang, W.J., et al., Impacts of freezing and thermal treatments on dimensional and mechanical properties of wood flour-HDPE composite. Forestry Research: English Edition, 2013, 24(1), 5. https://doi.org/10.1007/s11676-013-0334-0

[22] Zhu Y. et al., Experimental study on uniaxial compressive properties of parallel strand bamboo at high temperatures. Journal of Building Structures. 2021,42(09), 1-7. https://doi.org/10.14006/j.jzjgxb.2019.0866

[23] Xu, M., et al., Experimental study on compressive and tensile properties of a bamboo scrimber at elevated temperatures. Construction and Building Materials, 2017, 151, 732-741. https://doi.org/10.1016/j.conbuildmat.2017.06.128

[24] The European Standard EN 1995-1-2: 2004(E), Eurocode 5: Design of Timber Structures-Part 1-2: General. Structural fire design, 2004.